# Ionospheric delay estimation strategies using Galileo E5 signals only

Olivier Julien, Christophe Macabiau, Jean-Luc Issler

▶ **To cite this version:**

Olivier Julien, Christophe Macabiau, Jean-Luc Issler. Ionospheric delay estimation strategies using Galileo E5 signals only. GNSS 2009, 22nd International Technical Meeting of The Satellite Division of the Institute of Navigation, Sep 2009, Savannah, United States. pp 3128-3141. hal-01022161

**HAL Id: hal-01022161**

**https://enac.hal.science/hal-01022161v1**

Submitted on 30 Sep 2014

**HAL** is a multi-disciplinary open access archive for the deposit and dissemination of scientific research documents, whether they are published or not. The documents may come from teaching and research institutions in France or abroad, or from public or private research centers.

L'archive ouverte pluridisciplinaire **HAL**, est destinée au dépôt et à la diffusion de documents scientifiques de niveau recherche, publiés ou non, émanant des établissements d'enseignement et de recherche français ou étrangers, des laboratoires publics ou privés.

# Ionospheric Delay Estimation Strategies Using Galileo E5 Signals Only

Olivier Julien, Christophe Macabiau, Ecole Nationale de l'Aviation Civile, Toulouse, France
Jean-Luc Issler, Centre Nationale d'Etudes Spatiales, Toulouse, France

## BIOGRAPHIES

**Olivier Julien** is a researcher/lecturer at the signal processing laboratory of ENAC (Ecole Nationale de l'Aviation Civile – French Civil Aviation University), Toulouse, France. His research interests are GNSS receiver design, GNSS multipath and interference mitigation and GNSS interoperability. He received his engineer degree in 2001 in digital communications from ENAC and his PhD in 2005 from the Department of Geomatics Engineering of the University of Calgary, Canada.

**Christophe Macabiau** graduated as an electronics engineer in 1992 from the ENAC in Toulouse, France. Since 1994, he has been working on the application of satellite navigation techniques to civil aviation. He received his Ph.D. in 1997 and has been in charge of the signal processing lab of the ENAC since 2000.

**Jean-Luc Issler** is head of the Instrumentation Telemetry and Propagation department of the CNES Radio Frequency sub-directorate since august 2009. He is one of the CBOC inventors, and proposed the GALILEO E5 signal using the ALTBOC 8-PSK invention made by Laurent Lestarquit. He graduated first from the Ecole Supérieure d'Electronique de l'Ouest (ESEO). He received the Astronautic Prize of AAAF (French aeronautical and space association) in 2004, and the EADS Science and Engineering prize, delivered in 2008 by the French Academy of Sciences, for his work on GNSS frequencies and modulations, and spaceborne RF equipments.

## ABSTRACT

Future open Galileo signals on E1, E5a and E5b bands will provide measurements with reduced tracking errors thanks to their signal structure. Moreover, because they are located on different bands, they also allow for efficient ionospheric delay estimation. The consequence is an accurate positioning capability, even based on code-based pseudorange measurements. This article investigates the event of a triple-frequency Galileo receiver losing the Galileo E1 signal. In this case, ionospheric delay estimation becomes difficult since the E5a and E5b frequency bands are very close. Several methods are investigated for this purpose. It is seen that the use of a vertical Total Electron Content model to represent the ionosphere delay for all visible satellites is very promising. When included in a Kalman filter, it offers an ionospheric delay estimation accuracy at the sub-meter level with a convergence time of only a few minutes. An extension is then provided to the single-frequency case where only E5b is available. A slight degradation in accuracy and convergence time is obtained compared to the dual-frequency E5a/E5b case is observed, although the results are also promising.

## INTRODUCTION

Future Galileo open signals, E5 (E5A/E5B) and E1 OS, were designed so that they can bring significant improvements to the users compared to the current GPS L1 C/A signal performances. Galileo receivers will be able to track the different signals with a lower tracking noise, a lower multipath susceptibility, and an increased resistance to interferers. These enhancements were obtained thanks to, among others, the use of higher code chipping rates (10.23 MHz for E5A and E5B), innovative modulations (BOC, ALTBOC, MBOC) and the use of a pilot channel in parallel with the traditional data channel.

The use of the 3 Galileo open signals together can bring further obvious improvements such as (1) a more accurate and robust ionospheric delay estimation, (2) improved ambiguity resolution performances (in terms of success rate and time to fix), (3) potential tropospheric delay estimation, and (4) frequency diversity against potential intentional or unintentional jammers. These different points were backed up by many different investigations and papers from different user community needing high precision and reliable positioning, showing a great interest in a triple-frequency Galileo (and GPS) receiver.

An important point is that even if only code-based pseudorange measurements are used, it is still possible to obtain precise positioning at the meter-level. This is very important for a wide range of applications that do not want to rely exclusively on carrier-phase measurements for positioning.

Based on this triple frequency baseline, it is important when it comes to sensitive applications, to consider

degraded modes since it might impact the expected behavior of the receiver. A typical example is the loss of one frequency and it is thus important for a triple-frequency Galileo receiver to consider the loss of any of the E5A, E5B and E1 signal and its consequence on the performances [Issler et al, 2004].

This article specifically focuses on the event of the loss of the Galileo E1 frequency. This situation is of particular interest because it means that the receiver is left with measurements coming exclusively from E5A and E5B signals, which are spectrally very close and thus not ideal for ionospheric delay estimation. Many different figures of merit are to be investigated in this degraded mode scheme to fully assess how the receiver can cope without significantly losing any of its performance. However, this article will only focus on 1: the ionospheric delay estimation. The motivation behind this investigation is to show that for a triple frequency Galileo receiver, whatever the jammed band, it is always possible to estimate accurately the ionospheric delay affecting pseudorange measurements and thus to keep the accurate positioning ability of the receiver. Moreover, an extension of this point is the potential use of the E5 band alone for precise positioning applications. Two different user cases are assumed in the paper:

- the single-frequency case: the estimation of ionospheric delays is based on E5a or E5b signal,
- the dual-frequency user that can use both E5a and E5b observables.

In the first section, the Galileo E5 signals will be described, as well as their performance. Then, the carrier-phase and code observables will be introduced. Section 3 presents the simulation tool that will be used for testing. The fourth section will introduce the dual frequency case, showing the different options considered to estimate the ionospheric delay. Finally, before concluding, the single-frequency case will be presented.

## OVERVIEW OF GALILEO E5 SIGNALS

The Galileo E5 signals are part of the E5 band ([1164-1215 MHz] that is the largest RadioNavigation Satellite System (RNSS) band. It is also an Aeronautical RadioNavigation Service (ARNS) band, thus protected by ITU, but with no exclusivity to RNSS. This means that any system broadcasting within this band will have to cope with the existing non-RNSS services already present in this band. In particular, systems using strong pulsed signals, such as Distance Measuring Equipments (DME), TACtical Air Navigation (TACAN) are deployed in this band [RTCA, 2004; Bastide, 2004].

### *Galileo E5 Signal Specification*

The Galileo E5 signal has 2 components:

- The E5a signal is transmitted in the frequency band [1164 MHz – 1191.795 MHz] and centered on $f_{E5a}$=1176.45 MHz. It will fully support the Galileo Open Service (OS) and will support the Safety of Life (SoL) service through its ranging function. It is composed of a data and pilot channel with equal power. The data channel broadcasts the F/NAV message (corresponding to the OS) with a symbol rate of 50 sps. Since the useful data is encoded using a convolutional code with a constraint ½, the actual data bit rate is 25 bps. Galileo E5a is Quadra-Phase Shift Keying (QPSK) modulated and uses a 10230-chip long spreading code with a chipping rate $f_c$ of 10.23 MHz. This means that it is a wide-band signal that will exhibit excellent resistance towards thermal, multipath and narrow-band interference compared to the currently available GPS C/A signal. It is also worth noting that the Galileo E5a signal will overlap the GPS L5 signal, which has similar signal characteristics. It means that it will likely be part of GPS/Galileo receivers using the E5a/L5 frequency band.
- The E5b signal is transmitted in the frequency band [1191.795 MHz – 1215 MHz], centered on $f_{E5b}$=1207.14 MHz. The Galileo E5b signal will support the OS, the SoL full service (ranging and integrity functions) and the Commercial Service (CS). It is composed of data and a pilot channels with equal power. The data channel broadcasts the I/NAV message (corresponding to the SoL service) with a symbol rate of 250 sps This means a useful data bit rate of 125 bps due to the convolutional encoding with a constraint 1/2. Galileo E5b uses a 10230-chip long spreading code with a chipping rate $f_c$ of 10.23 MHz. Although the Galileo E5b does not coincide spectrally with any planned GPS signal, it has the same frequency and modulation as the future COMPASS B2 signal, which might be interoperable with Galileo E5b, and is very close to the future GLONASS L3 signal.

It can be seen that Galileo E5a and Galileo E5b are present in adjacent band. In order to take advantage of that, the 2 signals are transmitted coherently using an ALTBOC(15,10) modulation [Lestarquit et al., 2008]. The whole Galileo E5 signal is thus an extra wide-band signal (more than 50 MHz wide) that can be received:

- as a whole: this means that the user can process an extra-wide band signal for positioning, thus enjoying pseudorange measurements that are the most resistant GNSS signals towards thermal noise, multipath and narrow-band interference [Simski et al, 2006].
- separately: in this case, the user does not require a receiver with an extra-wide bandwidth, thus reducing the complexity of the receiver. Note that a dual frequency E5a/E5b receiver can process in parallel both signals, thus obtaining measurements from 2

wide-band signals that were generated based on the same satellite payload module (same filter with excellent stability over the E5 band, same HPA) at 2 different frequencies.

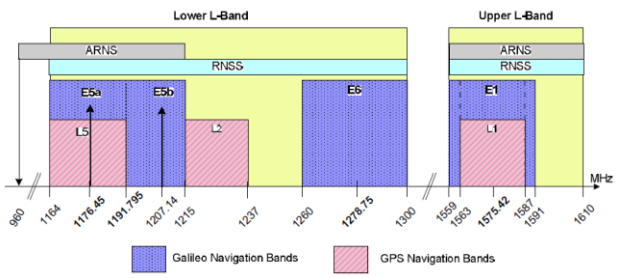


**Figure 1 – Galileo and GPS Spectral Occupation in the L-Band**

Compared to the Galileo E1 OS, and to a larger extend GPS L1 C/A, the Galileo E5a and E5b signals will provide enhanced tracking capabilities, and thus are very promising for precise positioning applications. Moreover, [Galileo SIS ICD, 2008] specifies that both Galileo E5a and E5b signals should be received with a minimum power 2 dB above the Galileo E1 OS. This also means a better performance in case of signal obstruction.

### *Galileo E5 Signal Performance*

Tracking of the future GNSS signals, including the Galileo E5 signals can be done based on the pilot channel only. The tracking noise standard deviation due to thermal noise can be approximated (assuming a wide-band filter) by:

$$\sigma_{P,noise} = \frac{c}{f_c}\sqrt{\frac{B_L^{DLL} d}{2\alpha \frac{C}{N_0}}\left(1+\frac{1}{\frac{C}{N_0}T_I}\right)}(m) \qquad \text{Eq.(1)}$$

$$\sigma_{\varphi,noise,X} = \frac{\lambda_X}{2\pi}\sqrt{\frac{B_L^{PLL}}{\frac{C}{N_0}}}(m) \qquad \text{Eq. (2)}$$

where

- $B_L^{DLL}$ and $B_L^{PLL}$ are the DLL and PLL equivalent loop filter bandwidths in Hz,
- $d$ is the DLL correlator spacing in chip,
- $T_I$ is the correlation time in s,
- $c$ is the speed of light in m/s,
- $\alpha$ is the slope of the normalized spreading sequence autocorrelation function in $d/2$,
- $\frac{C}{N_0}$ is the carrier to noise PSD ratio in dB-Hz, and
- $\lambda_X$ is the wavelength of signal $X$ in m.

Table 1 shows typical receiver settings for a wide-band receiver (24 MHz double sided for all signals except for Galileo E5 where an RF filter bandwidth of 50 MHs is considered).

**Table 1 – Typical Receiver Settings**

| | $B_L^{DLL}$ (Hz) | $d$ (Chips) | $T_I$ (ms) | $\alpha$ (Chip$^{-1}$) | $\lambda_X$ (m) |
|---|---|---|---|---|---|
| **L1 C/A** | 1 | 1/12 | 20 | 1 | 0.1903 |
| **E1** | 1 | 1/12 | 100 | 5.4 | 0.1903 |
| **E5a** | 1 | 1 | 100 | 1 | 0.2548 |
| **E5b** | 1 | 1 | 100 | 1 | 0.2483 |
| **E5** | 1 | 1/5 | 100 | 6.7 | 0.2515 |

Figure 2 shows the code and carrier-phase tracking noise obtained using Eq. (1) and (2) based on the receiver settings from Table 1. It can be seen that Galileo E5 provides a great improvement in terms of code measurement noise compared to other open signals.

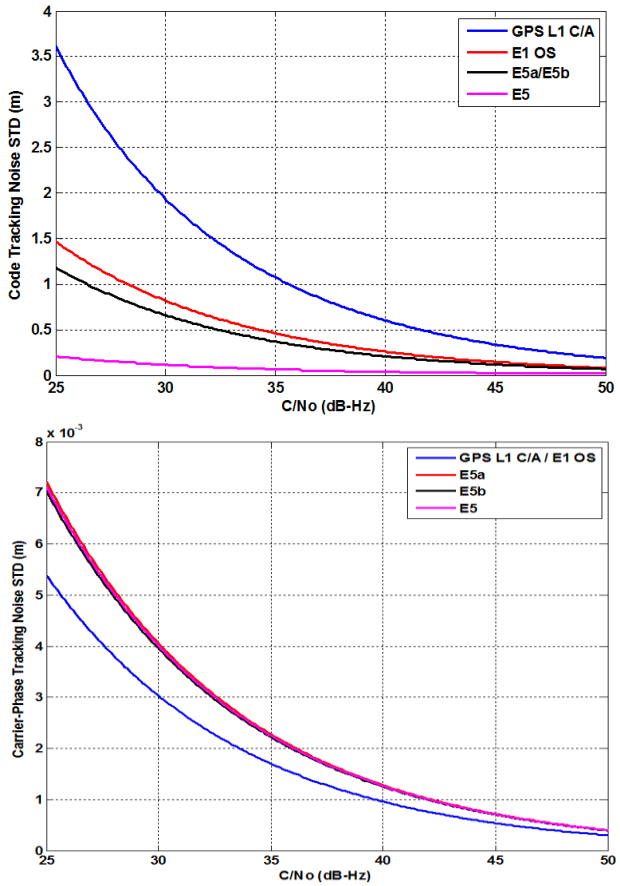


**Figure 2 – Code (Top) and Carrier-Phase (Bottom) Tracking Noise Using the Settings from Table 1**

The resistance of a signal against multipath is usually represented through the multipath envelope, which represents the worst tracking error assuming one multipath with a given amplitude, delay and phase with respect to the direct signal. The code and phase multipath envelopes are represented in Figure 3 for a multipath whose amplitude is half that of the direct signal.

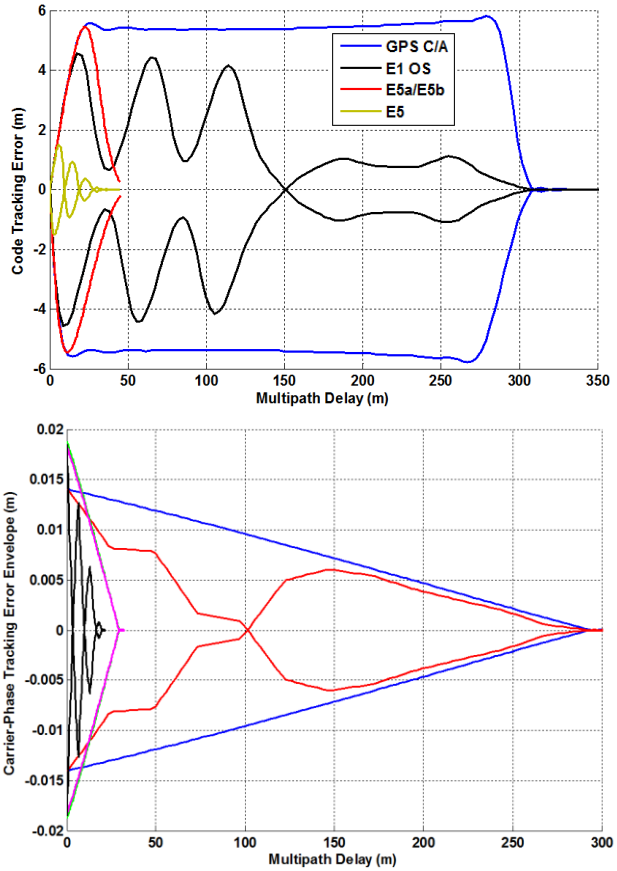


**Figure 3 – Code (Top) and Carrier-Phase (Bottom) Multipath Envelope Using the Settings from Table 1 and a Direct Signal-to-Multipath Amplitude Ratio of 2**

This analysis above showed that the Galileo E5a and E5b signals have tracking performances that are significantly better than GPS L1 C/A performance. They even outperform future open signals on the L1 band (such as Galileo E1 OS or GPS III L1C). They are thus very interesting to use for accurate positioning. In particular, the use of the whole Galileo E5 signal shows amazing performances.

## OBSERVABLE MODEL

Let us denote $P_X^{S_Y}$ and $\varphi_X^{S_Y}$ the code and carrier phase pseudorange measurements from satellite $S_Y$ at frequency $X$. Their usual model is provided by:

$$\begin{aligned} P_X^{S_Y}(k) = {} & \rho^{S_Y}(k) + d\rho^{S_Y}(k) \\ & + c\left(dT^{S_Y}(k) - dt^{S_Y}(k)\right) \\ & + T^{S_Y}(k) + I_X^{S_Y}(k) \\ & + MP_{P,X}^{S_Y}(k) + n_{P,X}^{S_Y}(k) \\ & + b_{P,X}^{S_Y}(k) \end{aligned} \qquad \text{Eq. (3)}$$

$$\begin{aligned} \varphi_X^{S_Y}(k) = {} & \rho^{S_Y}(k) + d\rho^{S_Y}(k) \\ & + c\left(dT^{S_Y}(k) - dt^{S_Y}(k)\right) \\ & + T^{S_Y}(k) - I_X^{S_Y}(k) \\ & + MP_{\varphi,X}^{S_Y}(k) + n_{\varphi,X}^{S_Y}(k) \\ & + b_{\varphi,X}^{S_Y}(k) + \lambda_X A_X^{S_Y} \end{aligned} \qquad \text{Eq. (4)}$$

where

- The superscript $S_Y$ refers to the satellite $S_Y$,
- $\rho$ represents the true satellite-receiver range,
- $d\rho$ represents the error associated with the uncertainty on the satellite antenna position,
- $dT$ represents the satellite clock bias,
- $dt$ represents the receiver clock bias,
- $T$ represents the tropospheric delay,
- $I_X$ represents the ionospheric delay at frequency $X$,
- $MP_P$ and $MP_\varphi$ represent the error due to multipath on the code and phase pseudoranges,
- $n_P$ and $n_\varphi$ represent the error due to thermal noise on the code and phase pseudoranges,
- $b_{P,X}^{S_Y}$ and $b_{\varphi,X}^{S_Y}$ represent the satellite+receiver code and phase biases at frequency $X$.
- $A_X$ represents the carrier phase ambiguity at frequency $X$,
- $\lambda_X$ represents the wavelength of the carrier $X$.

In order to gather the elements of Eq. (3) and Eq. (4) that are common to the different frequencies and observables of satellite $S_Y$, . (3) and Eq. (4) can be re-written as:

$$\begin{aligned} P_X^{S_Y}(k) = {} & D^{S_Y}(k) + I_X^{S_Y}(k) + MP_{P,X}^{S_Y}(k) \\ & + n_{P,X}^{S_Y}(k) + b_{P,X}^{S_Y}(k) \end{aligned} \qquad \text{Eq. (5)}$$

$$\begin{aligned} \varphi_X^{S_Y}(k) = {} & D^{S_Y}(k) - I_X^{S_Y}(k) + MP_{\varphi,X}^{S_Y}(k) \\ & + n_{\varphi,X}^{S_Y}(k) + b_{\varphi,X}^{S_Y}(k) \\ & + \lambda_X A_X^{S_Y} \end{aligned} \qquad \text{Eq. (6)}$$

where

$$\begin{aligned} D^{S_Y}(k) = {} & \rho^{S_Y}(k) + d\rho^{S_Y}(k) + c\left(dT^{S_Y}(k) - dt^{S_Y}(k)\right) \\ & + T^{S_Y}(k) \end{aligned}$$

It is well known that the ionospheric delay is frequency dependent. This dependence can be modeled, at the first order, by:

$$I_X^{S_Y}(k) = \frac{40.3 \cdot STEC^{S_Y}(k)}{f_X^2} \qquad \text{Eq. (7)}$$

where

- $f_X$ is the signal's carrier frequency, and
- $STEC$ is the Slant Total Electron Content (TEC), which represents the TEC along the signal propagation path.

Because of this dependence upon the carrier frequency, and due to the current use of GPS civil signal on the L1 frequency, this article will take the ionospheric delay at L1 as the reference ionospheric delay value. The

ionospheric delay at frequency $X$ can be translated into the ionospheric delay at the L1 frequency using:

$$I_{L_1}(k) = \gamma_X I_X(k) \quad \text{Eq. (8)}$$

with $\gamma_X = f_X^2 / f_{L_1}^2$.

The values of the coefficient $\gamma_X$ are shown in Table 2.

**Table 2 – Value of $\gamma_X$ as a function of the frequency used**

| Frequency | $\gamma_X$ |
|---|---|
| E1 | 1 |
| E5a | 0.56 |
| E5b | 0.59 |
| E5 | 0.57 |

This paper assumes that only ionosphere estimation is of interest to the user, and that position computation can be done based on a separate PVT computation (using the estimated ionospheric delay). Consequently, the measurements that will be used in the following study will all be geometry-free, which means that they will not depend upon the term $D$ present in Eq. (5) and Eq. (6).

## SIMULATION TOOL

This section introduces the parameters that are used to test the algorithms that will be proposed in the upcoming sections.

The user is assumed to be in Kourou, French Guyana since it is an area where ionospheric activity is generally higher than in Europe.

The assumed Galileo Medium Earth Orbit (MEO) constellation is composed of 27 satellites distributed over 3 equally spaced orbital planes inclined at 56° (each plane possesses 10 satellites, including 1 spare that is not used in this study). The orbits are circular with a radius of 29,600,318 m [EUROCAE, 2007].

Because the current Galileo OS Signal-In-Space (SIS) Interface Control Document (ICD) specifies performances down to a 10° elevation angle, it was assumed that the user had set a mask angle of 10°. Figure 4 shows the number of visible Galileo satellites on Jan 1st 2013.

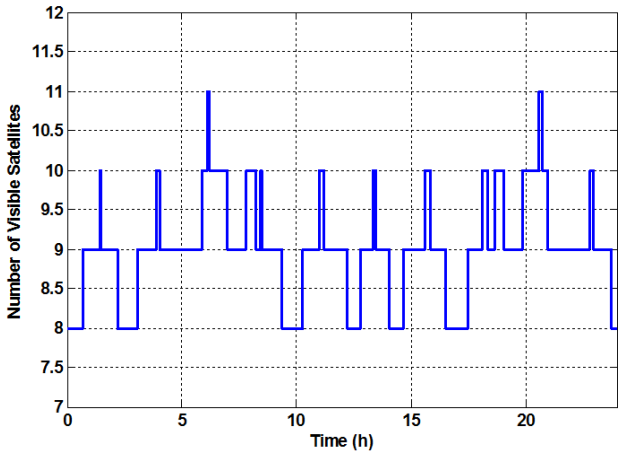


**Figure 4 – Number of Visible Satellites for a User Located in Kourou, French Guyana**

As it was expressed in the previous section, only geometry-free measurements will be used. As such the simulation tool only needs to model the remaining terms: the ionospheric delay, multipath-induced errors, thermal noise, satellite and receiver group and phase delays, and carrier-phase ambiguities.

The simulated ionospheric delay on L1 is based on the Klobuchar ionosphere model used by the GPS for ionosphere correction [Klobuchar, 1996]. Because such a correction will not be used by our algorithm, it was deemed appropriate for algorithm testing due to its wide use and simplicity. It is however acknowledged that further testing should be based on more recent and more accurate models such as the NeQuick model or the IRI 2007 [IRI, 2009],. The ionospheric delays at E5a and E5b frequencies are obtained using Eq. (8). Figure 5 shows the ionospheric delay at L1 corresponding to the same user conditions as in Figure 4.

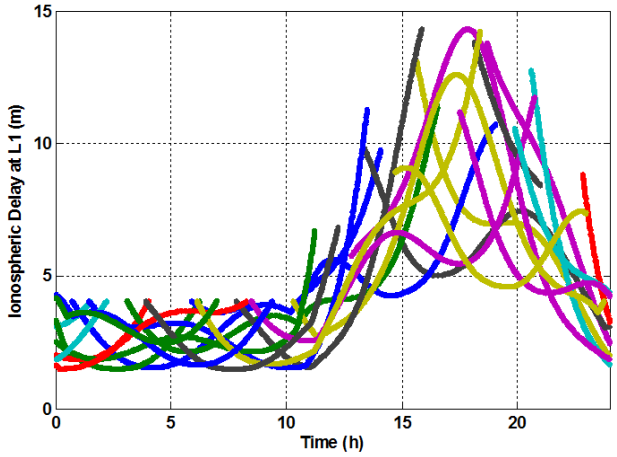


**Figure 5 –Simulated Ionospheric Delay at L1 for all the Satellites**

The simulated thermal noise effect is based on a Gaussian noise generator with a standard deviation provided by Eq.

(1) and (2), and using the receiver parameters provided in Table 1.

The multipath effect was difficult to model since no general model was found for all types of users at the measurement level. It was thus decided to use a very simple model based on a single reflection on the ground with an antenna assumed 2 meters above the ground. The error is computed assuming that the tracking loops have converged instantly. The resulting code tracking error is shown in Figure 6 as a function of the satellite elevation for SV17.

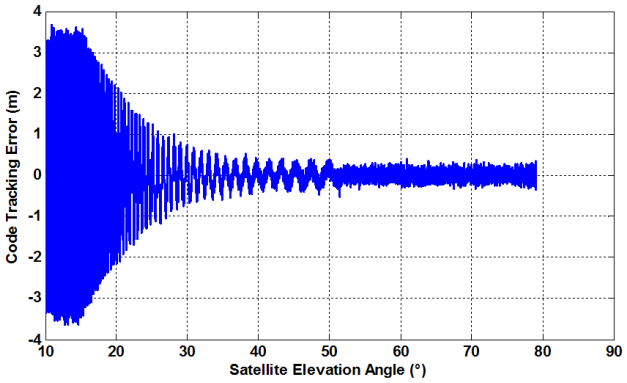


**Figure 6 – Multipath- and Noise-Induced Tracking Error on the Code Pseudoranges**

An estimated Galileo E5 link budget is based on [Rebeyrol, 2007]. Table 3 provides these key values. Remember that tracking is based on the use of the pilot channel only.

**Table 3 – Values used for Galileo E5 Link Budget Computation**

| | E5a | E5b | E5 |
|---|---|---|---|
| Transmitted power (dBW) | 18.92 | | |
| Payload losses (OMUX/filter/components, etc…) (dB) | 1.64 | | |
| Polarization losses (dB) | 1 | | |
| Atmospheric losses (dB) | 0.3 | | |
| Use of pilot tracking (dB) | -6 | -6 | -3 |

The satellite antenna gain pattern was chosen to be the same as the one used by the GPS Block IIR-M. The associated gain pattern can be found in [Chibout, 2008]. The receiver antenna gain pattern is compliant with the current EUROpean Civil Aviation Equipement (EUROCAE) Galileo Minimum Operational Performance Standards (MOPS) for an E1/E5 active antenna. In the same way, the $N_0$ value is based on current EUROCAE assumptions: -201.2 dBW/Hz. The resulting $C/N_0$ for the considered signal's component at the user antenna output is shown in Figure 7.

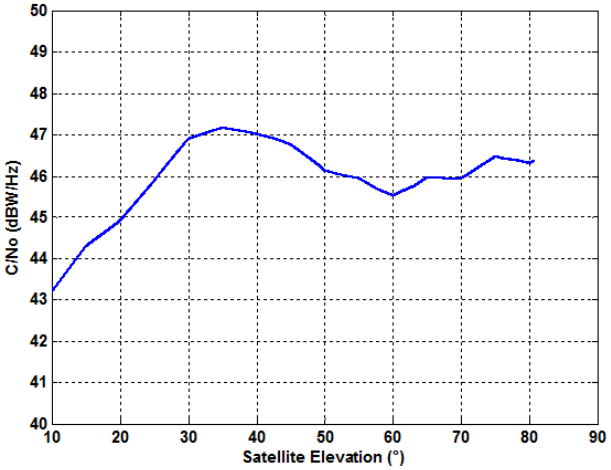


**Figure 7 – $C/N_0$ at the Antenna Output**

The group and phase delays are assumed equal to zero. The rationale behind this choice is the fact that the whole Galileo E5 signal is generated locally and passes through the same payload elements (filter, HPA, Output Multiplexer). This means that thermal variations affecting the Galileo E5a and E5b satellite group and phase delays will be coherent and stable. It is thus considered that the satellite bias can be entirely removed using the broadcast Galileo TGD. Regarding the receiver inter-frequency biases, it is assumed that they can be calibrated by the user.

Now that the simulation tool was introduced, the ionospheric delay estimation algorithms will be introduced and tested.

## DUAL-FREQUENCY USER

This section consists in testing several ionospheric delay estimation techniques based on the availability of Galileo E5a and E5b signals.

### *Code Pseudorange-Based Ionospheric Estimation*

When two signals available at 2 different frequencies are available, the ionospheric delay at L1 affecting the observables coming from one satellite can be directly estimated using the following combination:

$$\begin{aligned} \hat{I}_{L_1}^{S_Y}(k) &= \gamma_{X_1,X_2}\left(P_{X_1}^{S_Y}(k) - P_{X_2}^{S_Y}(k)\right) \\ &= I_{L_1}^{S_Y}(k) + k_{X_1,X_2} \\ &\cdot \left(MP_{P,X_1}^{S_Y}(k) - MP_{P,X_2}^{S_Y}(k)\right. \\ &+ n_{P,X_1}^{S_Y}(k) - n_{P,X_2}^{S_Y}(k) \\ &\left. + b_{P,X_1}^{S_Y}(k) - b_{P,X_2}^{S_Y}(k)\right) \end{aligned} \quad \text{Eq. (9)}$$

with

$$\gamma_{X_1,X_2} = \frac{\gamma_{X_1}\gamma_{X_2}}{\gamma_{X_2} - \gamma_{X_1}}$$

From Eq. (9), it can be seen that the estimated ionospheric delay at the L1 frequency $\hat{I}_{L_1}$ will be affected by thermal

noise, multipath coming from the code pseudoranges and inter-frequency biases. The level of this disturbance is directly proportional to the coefficient $\gamma_{X_1,X_2}$. The value of this coefficient is provided in Table 4 as a function of the frequencies used. It can be seen that the use of E5a and E5b signals provides a strong increase of the disturbance level (compared to the value of this coefficient for an E1/E5a combination). This was of course expected due to the vicinity of the E5a and E5b frequencies. The ionospheric delay estimation using Eq. (9) for an E1/E5b and an E5a/E5b combination can be observed on Figure 8 assuming no multipath. It can be seen that despite the better performance of E5a and E5b against thermal noise, the E1/E5b provides the best performance, by far. Note also that the simulation does not take into account the presence of inter-frequency biases, which would further increase the difference. Indeed, the existence of such errors would also be multiplied by the term $\gamma_{X_1,X_2}$. The presence of multipath is represented in Figure 9 and it can be seen that it provides an extremely bad estimation of the ionospheric delay based on E5a and E5b signals.

**Table 4 – Value of $\gamma_{X_1,X_2}$ as a function of the frequencies used**

| Combination | $\gamma_{X_1,X_2}$ |
|---|---|
| E1-E5a | 1.26 |
| E1-E5b | 1.42 |
| E1-E5 | 1.34 |
| E5b-E5a | 11.11 |

***Carrier-Smoothed Code Pseudorange-Based Ionospheric Estimation***

One way to reduce the noise level of $\hat{I}_{L_1}$ is to reduce the noise and multipath affecting code-based measurements. It is then very usual to use carrier-smoothing. The main filter to do so is known as the Hatch filter [Hatch, 1982]. It is given by:

$$\tilde{P}_{X_1}^{S_Y}(k) = \frac{1}{w} P_{X_1}^{S_Y}(k) + \left(1 - \frac{1}{w}\right) \cdot \left[\tilde{P}_{X_1}^{S_Y}(k-1) + \left(\varphi_{X_1}^{S_Y}(k) - \varphi_{X_1}^{S_Y}(k-1)\right)\right] \quad \text{Eq. (10)}$$

where

- $w = \begin{cases} k - k_0 \; if \; (k-k_0)\Delta t < T_{smoot\,h} \\ T_{smoot\,h} \; if \; (k-k_0)\Delta t \geq T_{smoot\,h} \end{cases}$
- $k_0$ represents the start time of the smoothing period,
- $T_{smoot\,h}$ is the filter time constant, and
- $\Delta t$ represents the measurement rate

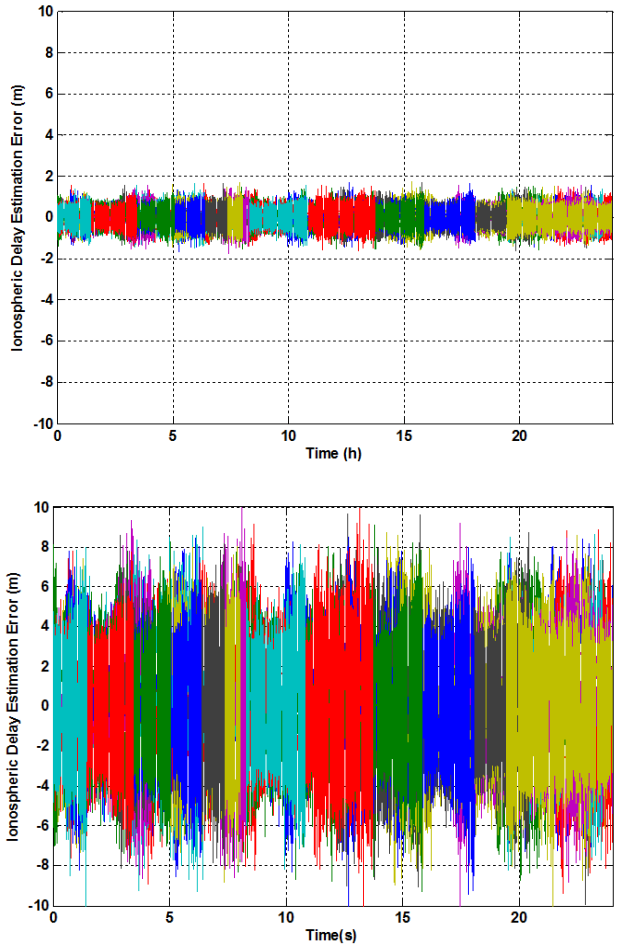


**Figure 8 – Ionospheric Delay Estimation Error Using Raw Code Pseudorange Dual-Frequency E1/E5b (Top) and E5a/E5b (Bottom) Combinations – no Multipath Considered**

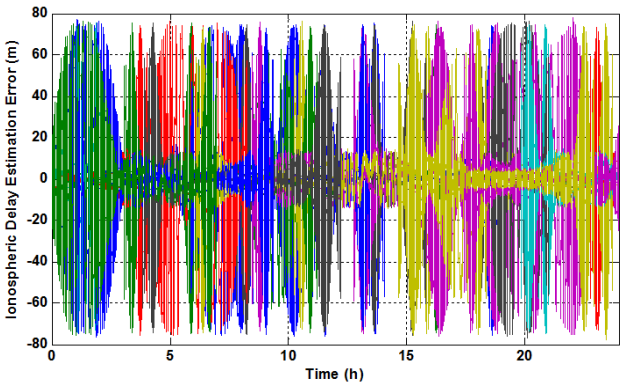


**Figure 9 – Ionospheric Delay Estimation Error Using Raw Code Pseudorange Dual-Frequency E1/E5b (Top) and E5a/E5b (Bottom) Combinations – with Multipath**

The advantage of carrier-smoothing is to provide an absolute code pseudorange that does not depend upon the carrier-phase ambiguity while having a significantly reduced measurement noise (reduces thermal noise and varying multipath-induced errors). It has however three main drawbacks for our purpose:

- The carrier-phase measurements have to be constantly checked in order to re-start the filter in case of cycle slip,
- The inter-frequency biases are kept since they are constant over the filter time constant,
- Since the ionospheric delay has an opposite sign on the code and carrier-phase pseudoranges, the resulting smoothed pseudorange ionospheric delay will not match the actual ionospheric delay. Indeed, it will be influenced by the rate of change of the ionospheric delay. In steady state, the filter divergence when the ionospheric delay varies at a rate of $V$ m/s over $T_{smoot\,h}$ sec is $-2V(w-1)$. This might not be a problem if the ionospheric delay estimate is injected in the carrier-smoothed pseudoranges though.

Figure 10 show the ionospheric delay estimation error using a 100-second smoothing filter (typical, for instance, of aeronautical users). The convergence process can be clearly seen every time a new satellite appears. The result is still quite strongly influenced by multipath, since even if a small residual multipath error is present after filtering, it will be multiplied by $\gamma_{X_1,X_2}$. This result has, however, to be taken with care since the multipath-induced error is generated in a simplistic way and assumes that the tracking loop has converged at each instant. This, for instance, means that the loop filtering effect is not taken into account and thus worsen the multipath error. Still, it can be seen that the method, by itself, might not be efficient in case of strong multipath. Interesting multipath mitigation techniques have been designed, such as [Axelrad et al, 1994], using the information from the estimated $C/N_0$. Because the E5a and E5b are generated coherently, efficient methods based on E5a and E5b signals could be used based on their relative phase offset and estimated $C/N_0$.

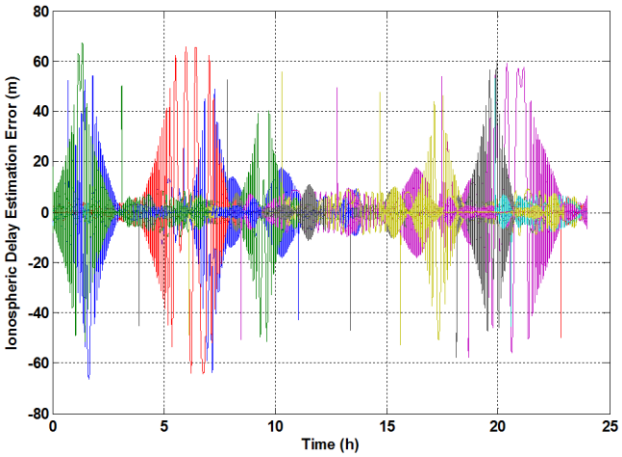


**Figure 10 – Ionospheric Delay Estimation Error Using Carrier-smoothed Code Pseudorange Dual-Frequency E1/E5b**

***Code and Carrier Pseudorange-Based Ionospheric Estimation***

To refine the ionospheric delay estimation, one would be tempted to use dual-frequency carrier-phase pseudorange measurements since they have a very limited tracking noise compared to code pseudoranges.

$$\begin{aligned}\hat{I}_{L_1}^{S_Y}(k)(k) &= \gamma_{X_1,X_2}\left(\varphi_{X_2}^{S_Y}(k)-\varphi_{X_1}^{S_Y}(k)\right)\\ &= I_{L_1}^{S_Y}(k)+\gamma_{X_1,X_2}\\ &\cdot\left(MP_{\varphi,X_1}^{S_Y}(k)-MP_{\varphi,X_2}^{S_Y}(k)\right.\\ &+ n_{\varphi,X_1}^{S_Y}(k)-n_{\varphi,X_2}^{S_Y}(k)\\ &+ \lambda_{X_1}A_{X_1}^{S_Y}-\lambda_{X_2}A_{X_2}^{S_Y}\\ &+ \left.b_{\varphi,X_1}^{S_Y}(k)-b_{\varphi,X_2}^{S_Y}(k)\right)\end{aligned} \quad \text{Eq. (11)}$$

Due to their intrinsic ambiguity term, the carrier phase measurements cannot, however, be used as such. This means that it is necessary to form a system with $2n$ observations ($n$ dual-frequency code measurements + $n$ dual-frequency carrier-phase pseudoranges) and $2n$ unknowns ($n$ ionospheric delays + $n$ float carrier-phase ambiguities). Such a system will likely take time to converge and might thus not be relevant for our purpose. Moreover, all code and phase measurements are not linked together in this technique when using geometry-free measurements. Indeed, the ambiguity term can be estimated only based on the code measurements coming from the same satellite. Thus, every time a new satellite appears, it will take time to estimate the associate carrier-phase ambiguity.

It might be interesting to use an ionospheric delay model that could reduce the number of ionospheric parameter to estimate and link all the available measurements so that the carrier-phase ambiguity of an appearing satellite would be more easily estimated in one update. Such an idea has been used for single-frequency (GPS C/A) ionospheric estimation in [Lestarquit et al. 1997; Moreno et al., 1999]. It has also been used for dual frequency GPS L1/L2 measurements in [Komjathy, 1997] in the context of Precise Point Positioning (PPP). The model assumes that the vertical TEC (VTEC) at any ionospheric pierce point can be modeled as a function of the VTEC at the user zenith and a linear function of the latitude and longitude of the pierce point relative to the user latitude and longitude. This can be written as:

$$\begin{aligned}\widehat{VTEC}(k) &= VTEC_u(k)\\ &+ \left(lat_u(k)-lat_p^{S_Y}(k)\right)\\ &\cdot g_{lat}(k)\\ &+ \left(long_u(k)\right.\\ &- \left.long_p^{S_Y}(k)\right)\cdot g_{long}(k)\end{aligned} \quad \text{Eq. (12)}$$

where

- $VTEC_u$ is the VTEC at the zenith of the user antenna,

- $g_{lat}$ *and* $g_{long}$ are the latitudinal and longitudinal VTEC gradients,
- $lat_u$ *and* $lat_p$ are the user and pierce point latitudes, and
- $long_u$ *and* $long_p$ are the user and pierce point longitudes.

This model might be of limited accuracy when there are local ionosphere activity, however, it has to be kept in mind that, assuming an ionosphere shell model at an altitude around 350 km, the location of the pierce points is within 9° in latitude and longitude from the user location (mask angle of 10° considered). This is equivalent to a square of approximately 2000 km in the East-West and North-South directions with the user at its center. The variation of the VTEC in this fairly reduced area could indeed, as a first approximation, be represented by a linear function assuming typical ionosphere activity.

Using a function that maps the VTEC value to an STEC value (mapping function), it is then possible to express the ionospheric delays from each satellite as a function of the 3 parameters $VTEC_u$ , $g_{lat}$ *and* $g_{long}$. A typical mapping function used by [Lestarquit et al, 1999] is:

$$MF^{S_Y}(k) = \frac{1}{\sqrt{1 - \left(\frac{R_e cos\left(E^{S_Y}(k)\right)}{R_e + h_I}\right)^2}} \qquad \text{Eq. (13)}$$

where

- $R_e$ is the Earth radius (6378.1363 km),
- $E$ is the satellite elevation (in rad), and
- $h_I$ is the height of the maximum TEC (~350 kms), which is also the height of the ionosphere layer.

The mapping function used by the Klobuchar model (and thus used to generate the ionospheric delay at L1 in the simulator) is:

$$MF_{Klob}^{S_Y}(k) = 1 + 16 \cdot \left(0.53 - \frac{E^{S_Y}(k)}{\pi}\right)^3 \qquad \text{Eq. (14)}$$

It is important to note that the mapping function shown in Eq. (13) is only an approximation of the mapping function used in the Klobuchar model (Eq. (14)).

Using Eq. (7), Eq. (12) and Eq. (13), the ionospheric delay at L1 can be modeled as:

$$\hat{I}_X^{S_Y}(k) = \frac{1}{\gamma_X}\Big(I_{V,L_1,u}(k) + \Delta lat^{S_Y}(k) G_{L_1,lat}(k) + \Delta long^{S_Y}(k) G_{L_1,long}(k)\Big) \qquad \text{Eq. (15)}$$

where

- $I_{V,L_1,u} = K^{S_Y} \cdot \frac{VTEC_{user}}{f_{L_1}^2}$
- $G_{L_1,lat} = K^{S_Y} \cdot g_{lat}$
- $G_{L_1,long} = K^{S_Y} \cdot g_{long}$
- $K^{S_Y} = 40.3 \cdot MF^{S_Y}$
- $\Delta lat^{S_Y}(k) = lat_u(k) - lat_p(k)$
- $\Delta long^{S_Y}(k) = long_u(k) - long_p(k)$

Using Eq. (11), the system to solve then becomes:

$$\begin{bmatrix} \Delta P_{X_1,X_2}^{S_1}(k) \\ \Delta P_{X_1,X_2}^{S_2}(k) \\ \dots \\ \Delta P_{X_1,X_2}^{S_n}(k) \\ \Delta\varphi_{X_2,X_1}^{S_1}(k) \\ \Delta\varphi_{X_2,X_1}^{S_2}(k) \\ \dots \\ \Delta\varphi_{X_2,X_1}^{S_n}(k) \end{bmatrix} = H \begin{bmatrix} I_{V,L_1,u}(k) \\ G_{L_1,lat}(k) \\ G_{L_1,long}(k) \\ A_{X_1,X_2}^{S_1} \\ A_{X_1,X_2}^{S_2} \\ \dots \\ A_{X_1,X_2}^{S_n} \end{bmatrix} + \begin{bmatrix} N_{P,X_1,X_2}^{S_1}(k) \\ N_{P,X_1,X_2}^{S_2}(k) \\ \dots \\ N_{P,X_1,X_2}^{S_n}(k) \\ N_{\varphi,X_1,X_2}^{S_1}(k) \\ N_{\varphi,X_1,X_2}^{S_2}(k) \\ \dots \\ N_{\varphi,X_1,X_2}^{S_n}(k) \end{bmatrix} \qquad \text{Eq. (16)}$$

with

$$H = \frac{1}{k_{X_1,X_2}} \begin{bmatrix} \bar{\bar{K}}_X(k) & \overline{\overline{\Delta lat}}(k) & \overline{\overline{\Delta long}}(k) & \bar{\bar{0}}_n \\ \bar{\bar{K}}_X(k) & \overline{\overline{\Delta lat}}(k) & \overline{\overline{\Delta long}}(k) & k_{X_1,X_2}\bar{\bar{I}}_n \end{bmatrix}$$

where

- $\bar{\bar{K}}_X(k) = \begin{bmatrix} K_X^{S_1}(k) \\ K_X^{S_2}(k) \\ \dots \\ K_X^{S_n}(k) \end{bmatrix}$, $\overline{\overline{\Delta lat}}(k) = \begin{bmatrix} \Delta lat^{S_1}(k) \\ \Delta lat^{S_2}(k) \\ \dots \\ \Delta lat^{S_n}(k) \end{bmatrix}$,

  $\overline{\overline{\Delta long}}(k) = \begin{bmatrix} \Delta long^{S_1}(k) \\ \Delta long^{S_2}(k) \\ \dots \\ \Delta long^{S_n}(k) \end{bmatrix}$,
- $\bar{\bar{0}}_n$ is a n-by-n zero matrix
- $\bar{\bar{I}}_n$ is a n-by-n identity matrix
- $\Delta P_{X_1,X_2}^{S_Y} = P_{X_1}^{S_Y} - P_{X_2}^{S_Y}$
- $\Delta\varphi_{X_2,X_1}^{S_Y} = \varphi_{X_2}^{S_Y} - \varphi_{X_1}^{S_Y}$
- $A_{X_1,X_2}^{S_1} = \lambda_{X_1} A_{X_1}^{S_Y} - \lambda_{X_2} A_{X_2}^{S_Y}$
- $N_{P,X_1,X_2}^{S_1}$ and $N_{\varphi,X_1,X_2}^{S_1}$ are the observation noise assumed Gaussian and elevation dependent.

The measurement error variance is elevation dependent. It was decided to use a measurement's covariance matrix that is $C/N_0$ dependent and that takes into account the multipath impact.

It is interesting to note that this method has the advantage to separate the inter-frequency bias from the ionospheric delay estimation since the bias will be absorbed by the (float) ambiguity state present in Eq. (11) once the filter has converged.

This system can be associated with a state model in order to be integrated in a Kalman filter to improve the estimation process. To do so, the ionosphere-related terms will be modeled as first-order Gauss-Markov processes with an infinite correlation time. Also, the Earth rotation has to be taken into account to update the vertical ionospheric delay between 2 consecutive update times.

This brings only a minor improvement in our case since the measurement rate is 1 Hz. However, it becomes necessary for higher measurement rates. The state model is then:

$$\begin{bmatrix} I_{V,L_1,u}(k+1) \\ G_{L_1,lat}(k+1) \\ G_{L_1,long}(k+1) \\ A^{S_1}_{X_1,X_2}(k+1) \\ A^{S_2}_{X_1,X_2}(k+1) \\ \dots \\ A^{S_n}_{X_1,X_2}(k+1) \end{bmatrix} = F \begin{bmatrix} I_{V,L_1,u}(k) \\ G_{L_1,lat}(k) \\ G_{L_1,long}(k) \\ A^{S_1}_{X_1,X_2}(k) \\ A^{S_2}_{X_1,X_2}(k) \\ \dots \\ A^{S_n}_{X_1,X_2}(k) \end{bmatrix} + \begin{bmatrix} \sigma_{VTEC} \cdot n_{VTEC} \\ \sigma_{G_{lat}} \cdot n_{G_{lat}} \\ \sigma_{G_{long}} \cdot n_{G_{long}} \\ 0 \\ 0 \\ \dots \\ 0 \end{bmatrix} \quad \text{Eq.(17)}$$

with

$$F = \begin{bmatrix} 1 & 0 & W_e & 0 & \dots & 0 \\ 0 & 1 & 0 & 0 & \dots & 0 \\ 0 & 0 & 1 & 0 & \dots & 0 \\ 0 & 0 & 0 & 1 & \dots & 0 \\ \dots & \dots & \dots & \dots & \dots & 0 \\ 0 & 0 & 0 & 0 & 0 & 1 \end{bmatrix}$$

where

- $\sigma_{VTEC}$, $\sigma_{G_{lat}}$, $\sigma_{G_{long}}$ are the standard deviation associated with the uncertainty of the model,
- $n_{VTEC}$, $n_{G_{lat}}$, $n_{G_{long}}$ are independent Gaussian noise with a unit variance, and
- $W_e$ is the Earth rotation rate (rad/s)

The chosen covariance matrix of the state transition model was set empirically to allow a variation of 0.5cm/s for the vertical ionosphere component and 0.5 cm/rad/s for the gradients.

Note that the system has to deal with a changing number of measurements (appearing and disappearing satellites). The initial state value is approximated thanks to the use of the Klobuchar model, assuming that the latitudinal and longitudinal gradients are zero. It is done by computing all the VTEC values at each satellite pierce point and average them.

A first test was done assuming that the user has the same parameters (mapping function, pierce point coordinates, etc…) as the Klobuchar model used to generate the ionospheric delay. Also, no multipath was generated. This test was intended to see the performance limit of the technique. The results are shown in Figure 11, Figure 12 and Figure 13. It can be seen that the ionospheric delay estimation error is always below 1 meter. The good performance of the technique is due to the fact that the filter convergence time is low (a few minutes), which means that the estimation is almost entirely based on carrier-phase measurements, which are very accurate compared to code measurements.

When visualizing the vertical ionospheric delay estimation error in Figure 12, the "Klobuchar shape" can be clearly distinguished. The vertical ionospheric delay estimation is accurate within 15 cm during the whole day with a standard deviation of about 5 cm.

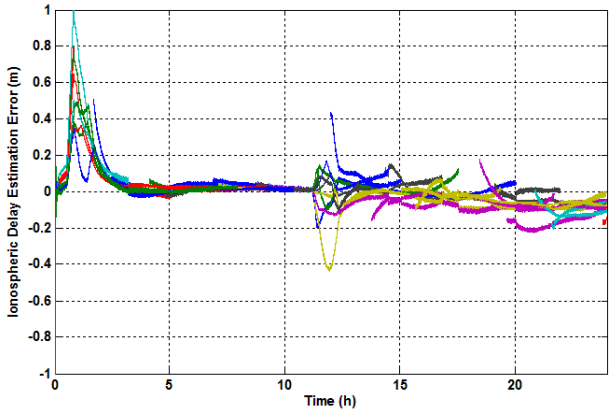


**Figure 11 – Ionospheric Delay Estimation Error using the Dual-Frequency Code/Phase Combinations**

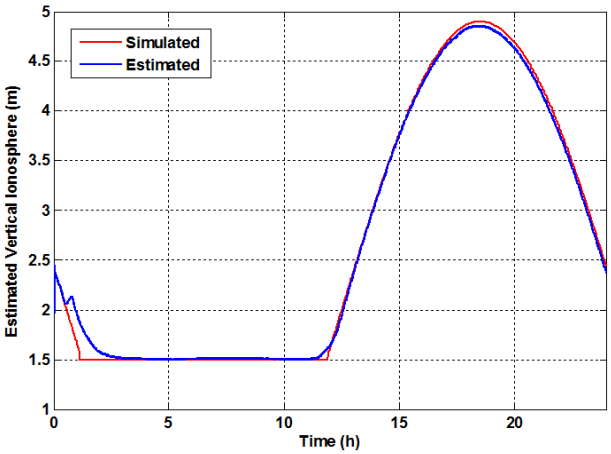


**Figure 12 – Vertical Ionospheric Delay Estimation Error using the Dual-Frequency Code/Phase Combinations**

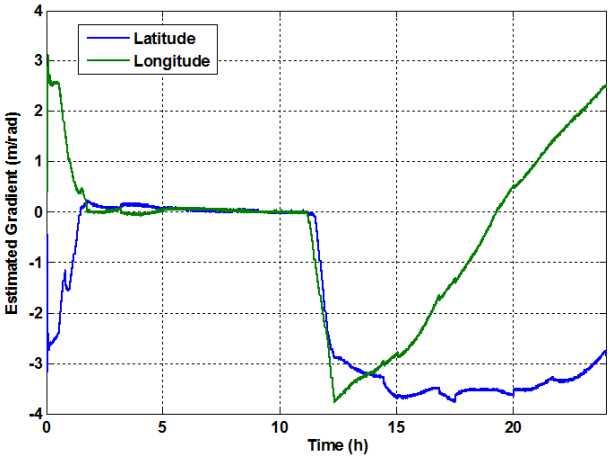


**Figure 13 – Latitudinal and Longitudinal Gradient Estimations using the Dual-Frequency Code/Phase Combinations**

The worst performance is reached when the ionospheric activity stops (around 01:30 – simulation time) and starts (around 12:00 – simulation time). Indeed, these are the periods of time when the vertical ionospheric model are the least linear, as it is represented in Figure 14. Also, during the active ionosphere period, the estimation process provides some errors mostly due to the satellite distribution (it can be seen in Figure 13 that the estimated gradients are affected by disappearing satellites).

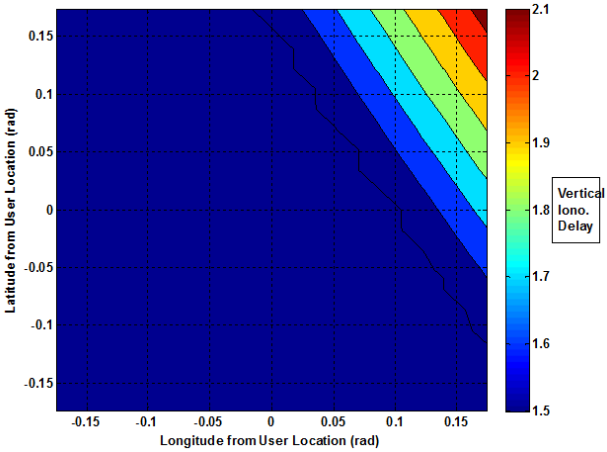


**Figure 14 – Vertical Ionospheric Delay at L1 at 12:30**

Because carrier-phase measurements are used to obtain Figure 11, it can be inferred that the figure represents the limitation coming from the vertical ionospheric model itself: it is not possible with this model and the provided satellite geometry to do better.

A second test was realized with multipath and the mapping function used in Eq. (13). The results are shown in Figure 15 and Figure 16 (note that there is an offset of 1 hour with respect to the previous data). It can be seen that the magnitude of the error has increased compared to Figure 11. However, it is still at the sub-meter level most of the time, which is very encouraging. The lines are thicker in Figure 11 due to the presence of the multipath whose induced error is multiplied by $\gamma_{X_1,X_2}$. It can also be seen that the deviation between the Klobuchar mapping function and the mapping function used in the system degrades the estimation process. Indeed, this deviation is higher for low-elevation satellites, and it is clear that it is appearing satellites that are disturbing the estimation process.

The estimated ionospheric delay is of excellent quality, as shown in Table 5 and Table 6. In particular, the standard deviation of the ionospheric delay estimation at L1 is within approximately 20 cm for all satellite elevations, and improves with increased satellite elevation.

It is clear that the obtained results are missing more testing with real ionosphere delays during high ionosphere activity. However, the results are very interesting because they show that the model is pushed to its limit and that thus Galileo E5a and E5b signals are providing the best possible results with this vertical TEC model.

The use of the Kalman filter allows good ionospheric delay estimation all the time, since the ionospheric delay of appearing satellites can be directly estimated from the vertical TEC model and thus the ambiguity is somewhat precisely estimated in one update. All available measurements can thus be used right away (which is not the case when using carrier-smoothing).

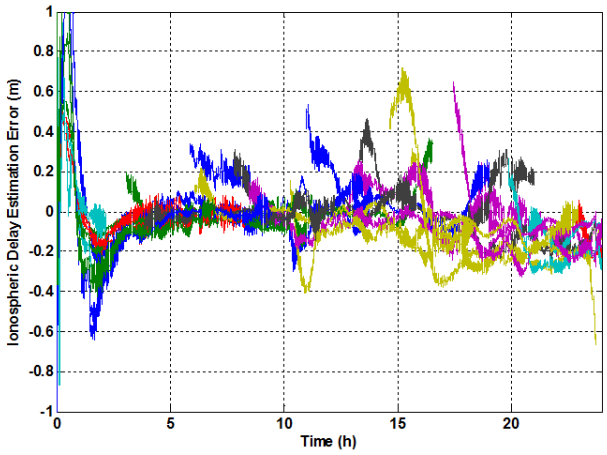


**Figure 15 – Ionospheric Delay Estimation Error using the Dual-Frequency Code/Phase Combinations**

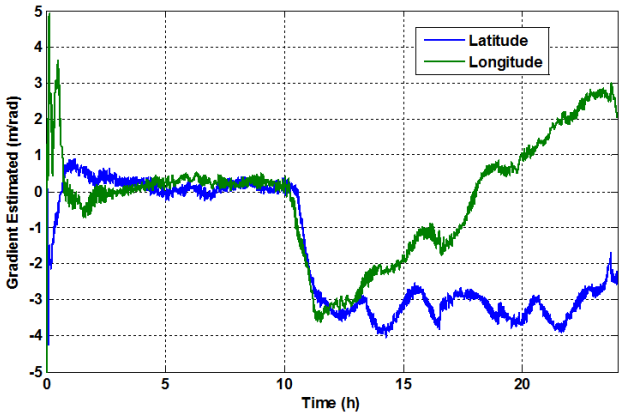


**Figure 16 – Latitudinal and Longitudinal Gradient Estimations using the Dual-Frequency Code/Phase Combinations**

## MONO-FREQUENCY CASE

In the case of a mono-frequency user, the only geometry-free measurement available is the Code-Minus-Carrier (CMC) measurement. Because the multipath- and noise-induced errors on the carrier phase measurements are significantly lower than that of the code pseudorange

measurements, the estimated ionospheric delay at L1 can be obtained from:

$$\begin{aligned}\hat{I}_{L_1}^{S_Y}(k) &= \frac{\gamma_X}{2} CMC_{X_1}^{S_Y}(k) \\ &= I_{L_1}^{S_Y}(k) \\ &+ \frac{\gamma_X}{2}\left(MP_{P,X_1}^{S_Y}(k)\right. \\ &+ n_{P,X_1}^{S_Y}(k) - \lambda_{X_1} A_{X_1}^{S_Y} \\ &\left.+ b_{P,X_1}^{S_Y}(k) - b_{\varphi,X_1}^{S_Y}(k)\right)\end{aligned} \qquad \text{Eq. (18)}$$

The CMC measurements are dependent upon the carrier phase ambiguity, which need to be estimated. Using the same vertical TEC model as the one used previously, It is clear that the system to solve will be close to that of the dual-frequency code/phase system represented in Eq. (16) and Eq. (17). The main difference is the use, as observations, of the CMCs only. The system will thus not be detailed herein.

The results are shown in Figure 17 and Figure 18 assuming that only the E5b signal is available. The ionospheric delay estimation noise at L1 is significantly increased compared to the dual-frequency case. This is mostly due to the fact that the CMC measurement noise are coming from code measurements, which are significantly higher than that of the carrier-phase measurements. Still, except during the convergence time, where errors can reach tens of meters, the ionospheric delay estimation error remain at the meter level, which is acceptable for the applications using code-based measurements for positioning. The convergence time of the filter is approximately twice that of the dual-frequency case.

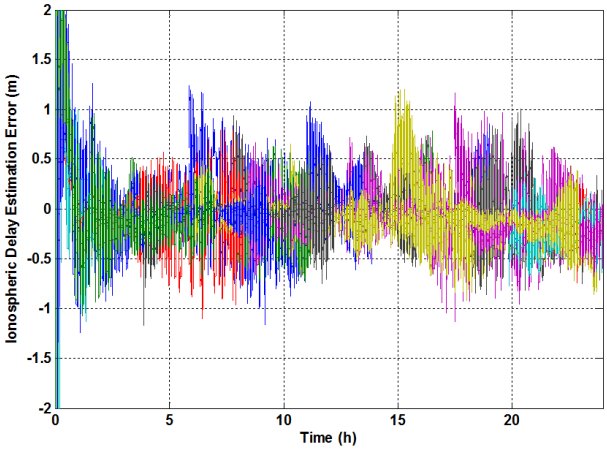


**Figure 17 – Ionospheric Delay Estimation Error for the Mono-Frequency Case**

From Figure 18, it can be seen that the estimation of the vertical ionospheric delay is quite good, while the latitude and longitude gradients become very noisy. This is due to the fact that the gradients are less observable and also means that better performance would be achieved if more satellites would be visible, or if dual-constellation was considered. It is clear that the noisy estimation of the gradients is the main source of error in the ionospheric delay estimation process. The ionospheric delay estimation error performance at L1, in terms of standard deviation and maximum error, is shown in Table 5 and.

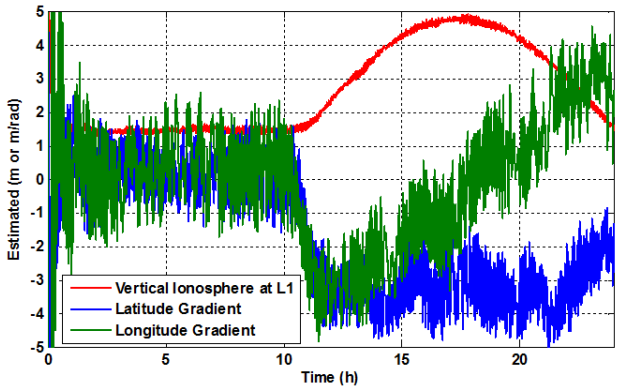


**Figure 18 – Vertical Ionospheric Delay, Latitudinal and Longitudinal Gradient Estimations for the Mono-Frequency Case**

This technique, however, shows that efficient ionospheric delay estimation can be achieved with a high quality single-frequency code measurement such as Galileo E5b. Obviously, the results would degrade with a more challenging ionospheric delay variation, which would be less "linear". However, assuming a typical ionosphere activity, the results are encouraging.

## CONCLUSIONS AND FUTURE WORK

The investigation has shown that very good ionospheric delay estimation could be achieved using Galileo E5 signals only, for both the single and dual-frequency cases.

Regarding Galileo E5a/E5b dual frequency users, the drawback due to the vicinity of the Galileo E5a and E5b was reduced thanks to 2 techniques. The first one is the use of carrier-smoothing that allows reducing the code pseudorange thermal noise- and multipath-induced errors. This method showed that, if bias-like errors remain after filtering, it can still result in very large errors. The second technique is based on the use of code and carrier-phase dual frequency measurements and a simple linear VTEC model to represent the VTEC at the ionospheric pierce point of each satellite in view. It thus requires the estimation of the dual-frequency carrier-phase ambiguities, of the vertical ionospheric delay at the user zenith and of the latitude and longitude gradients. It was shown that the estimated ionospheric delays were excellent (at the sub-meter level) with a convergence time of a few minutes only. This is mostly due to the reliance of the estimation process on the carrier-phase measurements. It also showed that the limiting factor of the technique was the vertical TEC model simplicity. More advance ionospheric models could be used, but the limited number of satellites in view makes it difficult to implement. It might be interesting in this case to consider

measurements made thanks to Galileo and at least another GNSS.

Regarding the mono-frequency case, the same vertical TEC model as for the dual-frequency case was used with the difference that CMC measurements were now used as observations. It was shown to provide good results, although noisier than in the dual frequency case. It also highlighted that the estimation of the latitude and longitude gradients was the weak point of the estimation process.

Future work includes:

- using of a more advanced multipath-induced error model (it is envisioned to simulate the actual code and carrier-phase tracking loops)
- designed a more efficient ionosphere model to try to improve the ionospheric delay estimation,
- testing of the proposed technique with a more advanced simulated ionospheric model (IRI 2007, NeQuick) during more challenging ionosphere activity and in more diverse locations. Still, it is worth to mention that the Klobuchar model, at the beginning and end of the "active" ionosphere provide very non-linear VTEC values. Thus, the obtained results are encouraging.
- including a cycle slip detector required to be able to use phase measurements,
- testing of the proposed technique for specific applications such as civil aviation, taking into account the actual expected performances.

## REFERENCES


Axelrad, P, C. Comp, and P. MacDoran (1994), *Use of Signal-to-Noise Ratio for Multipath Error Correction in GPS Differential Phase measurements: Methodology and Experimental Results*, Proceedings of the 1994 ION GPS Conference (Salt Lake City, UT, USE, Sept. 20-23), pp. 655-666.

Bastide, F. (2004), *Analysis of the Feasibility and Interests of Galileo E5a/E5b and GPS L5 Signals for Use with Civil Aviation*, PhD Dissertation, Institut National Polytechnique de Toulouse, France

EUROCAE (2008), *Interim Minimum Operational Performance Specification for Airborne Galileo Satellite Receiving Equipment* v0.26.

International Reference Ionosphere (2009), website http://ccmc.gsfc.nasa.gov/modelweb/models/iri_vitmo.php

Lestarquit, L. N. Suard, and J.-L. Issler (1997), *Determination of the Ionospheric Error using only L1 Frequency GPS Receiver*, Proceedings of the 1997 ION National Technical Meeting (Santa Monica, CA, Jan 14-16), pp. 313-322.

Moreno, R., N. Suard (1999), Ionospheric delay using only L1: validation and application to GPS receiver calibration and to inter-frequency biases estimation, Proceedings of the 1999 ION National Technical Meeting (San Diego, CA, Jan. 25-27), pp. 119-125.

Gao, G. X., S. Datta-Barua, T. Walter, and P. Enge (2007), *Ionosphere Effects for Wideband GNSS Signals*, Proceedings of the 63rd ION Annual Meeting (Cambridge, Massachusetts, April 23 - 25), pp. 147-155.

Hatch, R.R. (1982). The Synergism of GPS Code and Carrier Measurements. *Proceedings of the Third International Geodetic Symposium on Satellite Doppler Positioning*, New Mexico, II, pp. 1213-1232.

Issler J-L., L. Ries, J-M. Bourgeade, L. Lestarquit and C. Macabiau (2004), *Probabilistic Approach of Frequency Diversity as Interference Mitigation Means*. Proceedings of the 2004 ION GNSS Conference (Long Beach, CA, Sept. 21-24), pp. 2136-2145.

Komjathy, A. (1997), *Global Ionospheric Total Electron Content Mapping Using the Global Positioning System*. Ph.D. dissertation, Department of Geodesy and Geomatics Engineering Technical Report No. 188, University of New Brunswick, Fredericton, New Brunswick, Canada, 248 p.

Ouzeau, C., C. Macabiau, B. Roturier, M. Mabilleau, L. Azoulai, J. Levan, F. Besse (2008), *Ionospheric Delay Estimation In a Single Frequency Mode for Civil Aviation*, Proceedings of the 2008 ION GNSS Conference (Savannah, GA, USA, Sept. 16-19), pp.

Rebeyrol, E. (2007), *Galileo Signals and Payload Optimization*, PhD dissertation, Ecole Nationale Supérieure des Télécommunications, France

RTCA (2004), *DO292 - Assessment of Radio Frequency Interference Relevant to the GNSS L5/E5A Frequency Band*.

Simski, A, J.-M. Sleewaegen, M. Hollreiser, and M. Crisci (2006), *Performance Assessment of Galileo Ranging Signals Transmitted by GSTB-V2 Satellites*, Proceedings of the 1992 Institute Of Navigation GPS Conference (Albuquerque, NM, Sept. 16-18), pp. 483-490.

Xia, R. (1992) *Determination of Absolute Ionospheric Error Using a Single-Frequency GPS Receiver*, Proceedings of the 2006 Institute Of Navigation GNSS Conference (Fort Worth, TX, Sept. 26-29), pp. 1547-1559.

**Table 5 – Ionospheric Delay Estimation Error Standard Deviation at L1 for the Tested Techniques as a function of the Satellite Elevation**

| Standard Deviation of the Ionospheric Delay Estimation Error at L1 | Satellite Elevation Angle (°) | | | | | | | |
|---|---|---|---|---|---|---|---|---|
| | 10-20 | 20-30 | 30-40 | 40-50 | 50-60 | 60-70 | 70-80 | 80-90 |
| Dual Freq E5a/E5b using Iono Model | 0.21 | 0.11 | 0.11 | 0.10 | 0.05 | 0.05 | 0.08 | 0.05 |
| Mono-Freq E5b using Iono Model | 0.37 | 0.20 | 0.15 | 0.13 | 0.08 | 0.07 | 0.10 | 0.07 |

**Table 6 – Ionospheric Delay Estimation Maximum Error at L1 for the Tested Techniques as a function of the Satellite Elevation**

| Standard Deviation of the Ionospheric Delay Estimation Error at L1 | Satellite Elevation Angle (°) | | | | | | | |
|---|---|---|---|---|---|---|---|---|
| | 10-20 | 20-30 | 30-40 | 40-50 | 50-60 | 60-70 | 70-80 | 80-90 |
| Dual Freq E5a/E5b using Iono Model | 1.35 | 0.42 | 0.82 | 0.62 | 0.17 | 0.18 | 0.43 | 0.01 |
| Mono-Freq E5b using Iono Model | 2.15 | 0.79 | 1.16 | 0.79 | 0.33 | 0.27 | 0.57 | 0.09 |